Geoid and topography of Venus in various thermal convection models

NINA BENEŠOVÁ AND HANA ČÍŽKOVÁ

Department of Geophysics, Faculty of Mathematics and Physics, Charles University in Prague, V Holešovičkách 2, 180 00 Praha 8, Czech Republic (benesova@karel.troja.mff.cuni.cz)

Received: August 31, 2011; Revised: January 28, 2012; Accepted: February 7, 2012

ABSTRACT

Important though indirect information about the internal structure of Venus is provided by its topography and geoid. In the last decades this information has been used to constrain the Venus mantle viscosity structure and its dynamic regime. Recently, the geodynamic inversion of the Venus' geoid and topography resulted in a group of best fitting viscosity profiles. We use these viscosity models here as an input to our mantle convection code. We carry out simulations of the Venus' mantle evolution in a 3D spherical shell with depth dependent viscosity and check whether the character of the dynamic topography and the geoid represented by their power spectra fits the observed quantities. We compare the results with several other models obtained for different viscosity stratifications (constant, constant with highly viscous lithosphere, linear increase of viscosity). Further, we estimate the effect of other factors such as internal heating and varying Rayleigh number. We use a 2D spherical axisymmetric convection code to study the effect of lateral viscosity variations. In these 2D models we monitor the topography and the geoid developing above the axisymmetric plume and compare them with the observed elevations of Venus' geoid and topography in several Regia. Though none of the models fits observed data perfectly, we can generally conclude, that the best fit between the observed and predicted quantities is reached for viscosity profiles with 200 km thick lithosphere followed by a gradual increase of viscosity with depth and with the upper mantle viscosity of 2×10^{21} Pa s. For all viscosity profiles the predicted geoid and topography spectra match the observed ones only up to the degree 40, thus indicating other than dynamic origin of these quantities for higher degrees.

Keywords: geoid and topography, plumes, viscosity stratification of Venus

1. INTRODUCTION

As a sister planet of the Earth, whose dynamic processes should be controlled by the same physical processes, Venus has received a lot of attention from the mantle convection modellers (e.g. *Tackley, 1993*; *Steinbach and Yuen, 1994*; *Ratcliff et al., 1995*; *Schubert et al., 1997*; *Kiefer and Kellog, 1998*; *Steinbach and Yuen, 1998*; *Dubuffet at al., 2000*; *Choblet and Sotin, 2000*; *Yoshida and Kageyama, 2006*; *Běhounková and Choblet, 2009*; *Armann and Tackley, 2010*). As we have no direct information about the internal structure

of the Venus' mantle, the most important data that could constrain mantle processes are the surface topography and the geoid. Numerous studies have used this observation to constrain the mechanisms that maintain the topographic features. The possible mechanisms include isostasy (e.g. *Smrekar and Phillips, 1991*; *Arkani-Hamed, 1996*), elastic exure (e.g. *Barnett et al., 2002*) and mantle flow induced by density inhomogenities (e.g. *Kiefer et al., 1986*; *Simons et al., 1994*; *Pauer et al., 2006*; *Steinberger et al., 2010*). *Pauer et al. (2006)* have performed the geodynamic inversion of the geoid and topography data in order to estimate the viscosity stratification of the Venus' mantle. Using a rather simplifying assumption, namely that the mass anomaly distribution does not vary with depth, they concluded, that the geoid and topography spectra between the degrees 2 and 40 can be well explained by a whole mantle flow model. One of their best fitting five-layer viscosity profiles has a relatively high-viscosity lithosphere (about 2 orders of magnitude difference with respect to the upper mantle) and shows a gradual increase of viscosity with depth by a factor of 40 in the underlying mantle.

Since the early nineties, the relationship between the topography and the geoid has been studied in the framework of the numerical models of thermal convection in the Venus' mantle. The regional scale models of a single plume were used to put the first constraints on the mantle viscosity distribution on Venus. *Kiefer and Hager (1991)* tried to fit the geoid and topography of four selected plumes in a model with a depth dependent viscosity and concluded that their preferred model shows a moderate increase of viscosity in the lower mantle. Furthermore, they reported a trade-off between the viscosity increase and the Rayleigh number (*Ra*) - the model with a lower *Ra* and a viscosity increase gave the same fit as the model with a higher *Ra* and constant viscosity beneath the lithosphere. *Smrekar and Parmentier (1996)* studied the time evolution of the geoid and the geoid-to-topography ratio (GTR) in a similar model but with temperature dependent viscosity. They concluded that both quantities change with time and they used the GTR to estimate the evolutionary stage of several plumes on Venus. The effect of temperature dependent viscosity on the plume evolution and the predicted GTR were also studied by *Solomatov and Moresi (1996)* in a Cartesian model. They needed a rather thick lithosphere (200–400 km) to predict an average observed GTR and, for some plume regions, their stagnant lid was as thick as 500 km. Their preferred model was characterized by the *Ra* of 3×10^7. A relatively thick highly viscous lithosphere (about 200 km) is also consistent with the findings of *Reese et al. (1999)*.

Though efficient, the Cartesian or cylindric models of a single plume may suffer from incorrect geometry. It has been pointed out by *King (1997)* that the predicted geoid could vary by about 50% among the di_erent model geometries (cylindrical, Cartesian and spherical axisymmetric). Therefore the spherical models - axisymmetric (e.g. *Kiefer and Kellog, 1998*) or even fully 3D (e.g. *Yoshida and Kageyama, 2006*) are important in interpreting the geoid and topography data. Another advantage of these global models is the interaction of the plumes with the background mantle flow and a smaller dependence on the initial conditions. On the basis of 3D calculations with temperature dependent viscosity, *Yoshida and Kageyama (2006)* required a viscosity contrast of about 5 orders of magnitude over the mantle plus a step-wise increase in viscosity at the upper-lower mantle boundary to produce a stagnant lid convection with a realistic number of plumes. Their

geoid spectra correspond to the observed ones for a small viscosity jump at the upper-lower mantle boundary.

Viscosity is clearly the key parameter controlling the dynamic regime of the mantle, number of plumes etc. and its knowledge is crucial for understanding the relationship between the dynamic topography and the geoid. We study here this relationship systematically in a large group of models with various viscosity profiles and varying several other flow model parameters. Using 3D spherical simulation of thermal convection in a model with depth-dependent viscosity we test whether the spectra of our predicted geoid and topography correspond to the observed ones. We compare the results obtained for convection runs with different viscosity profiles (profiles from *Pauer et al. (2006)*, isoviscous mantle, constant viscosity mantle with a highly viscous lithosphere, linearly increasing viscosity) and test the effect of Rayleigh number. Besides the fit of the spectra, we also compare the characteristic flow patterns (namely the number of plumes developed). Further, in a 2D spherical axisymmetric model, that allows much more efficient calculations than the 3D model, we study the effect of lateral viscosity and internal heating. In the 2D models, we test not only the geoid and topography spectra, but also the evolution of the plumes developed at the pole and we compare their geoid and topography with the observations at selected upwelling structures on Venus.

When the time-dependent convection models are considered, an important question arises, how to compare the model results with the observations. The observed geoid and topography represent one snapshot of the system evolution. As the characteristics of the models may vary with time significantly, it is not clear which snapshot of the model run should be used for the comparison with the observed data. *Kiefer and Kellog (1998)* have shown in a 2D model that the time-dependent convection generates substantial variations of the geoid and topography in time and it may be therefore difficult to use these quantities to constrain the parameters like *Ra* and acceptable profiles of mantle viscosity. Therefore, rather than looking on the correspondence between the observed and predicted data at one time instant, we will present here the time averages of the L_2-norm differences in the models, where these quantities change with time substantially.

2. MODEL DESCRIPTION

Thermal convection in the mantle of Venus is described by the set of equations based on conservation of mass, momentum and energy. In incompressible extended Boussinesq approximation and neglecting inertial forces (e.g. *Matyska and Yuen, 2007*) we have continuity equation, momentum equation and heat equation as follows:

$$\nabla \cdot \boldsymbol{v} = 0\,, \tag{1}$$

$$\nabla \cdot \tau + \rho g = 0\,, \tag{2}$$

$$\frac{\partial T}{\partial t} = \nabla \cdot \left(\kappa \nabla T\right) - \boldsymbol{v} \cdot \nabla T - \frac{1}{c_p} v_r \alpha T g + \frac{1}{c_p \rho_0} \sigma : \nabla \boldsymbol{v} + \frac{Q_v}{\rho_0 c_p}\,. \tag{3}$$

Here $\boldsymbol{v}$ is the flow velocity, τ is the stress tensor, σ is the deviatoric part of the stress tensor, ρ is the density, g is the gravity acceleration, t is the time, v_r is the radial

component of velocity, c_p is the specific heat at constant pressure, T is the temperature, κ is the thermal diffusivity, ρ_0 is the reference density, α is the thermal expansivity and Q_v is the internal heating rate. Terms on the right hand side of Eq.(3) represent heat conduction, heat advection, adiabatic heating/cooling, viscous dissipation and internal (radioactive) heating, respectively. We assume a Newtonian approximation of mantle material: (radioactive) heating, respectively. We assume a Newtonian approximation of mantle material:

$$\tau = -p\mathbf{I} + \eta\left(\nabla \boldsymbol{v} + \nabla^T \boldsymbol{v}\right), \tag{4}$$

where p is the pressure, $\mathbf{I}$ is the identity tensor and η is the viscosity. Linearized equation of state gives the density as a function of temperature variations:

$$\rho = \rho_0\left[1 - \alpha\left(T - T_0\right)\right], \tag{5}$$

where T_0 is a reference temperature corresponding to the reference density ρ_0. In thermal equation (3) the dissipation term was omitted in 3D models to avoid aditional computational costs.

We solve the set of Eqs.(1)–(5) on a 3D spherical or 2D axisymmetric domain bounded by the core-mantle boundary (CMB) at the bottom and the surface at the top. On both of them we prescribe impermeable free-slip boundary conditions. Constant temperatures T_{top} and T_{cmb} are prescribed on the top and bottom surfaces, respectively. In the models where the effect of internal heating is included, the rate of Q_v ensures that the internal heating accounts for about 50% of the total surface heat ux. In some models, the buoyancy effect of the endothermic phase transition at a depth of 730 km is included using anomalous thermal expansivity (*Matyska and Yuen, 2007*). For values of the model parameters used see Table 1.

The style of convection depends on the mantle parameters whose joint influence can be characterised by a single dimensionless parameter - the Rayleigh number:

$$Ra = \frac{\rho_0 \alpha g\left(T_{cmb} - T_{top}\right) d^3}{\kappa\eta}, \tag{6}$$

where d is the thickness of the mantle. In the models with spatially variable viscosity, it is necessary to define which value of viscosity is to be used in the definition of Ra. The surface viscosity is often used for that purpose, here, however, that choice would be misleading, as we consider a high viscosity lid on the top in most of our calculations. Therefore, we use a volume average mantle viscosity and show the average Ra.

An initial temperature distribution was obtained by executing a run in a model with a relatively low Rayleigh number of 10^5 and a uniform viscosity. After reaching the statisticaly steady state, temperature distribution was used as an initial condition of subsequent model runs with variable viscosity and varying Ra. All results presented in this paper are taken after the system reached a statistically steady state with constant mean Nusselt number.

Table 1. Model parameters for Venus (*Yoshida and Kageyama, 2006*; *Schubert et al., 2001*).

Parameter	Symbol	Value	Units
Radius of Venus	r_{top}	6050	km
Core radius	r_{cmb}	3110	km
Gravity acceleration	g	8.6	$m\ s^{-2}$
Reference density	ρ_0	4200	$kg\ m^{-3}$
Coefficient of thermal expansion	α	2.5×10^{-5}	K^{-1}
Specific heat at constant pressure	c_p	1200	$J\ kg^{-1}\ K^{-1}$
Thermal diffusivity	κ	5×10^{-7}	$m^2 s^{-1}$
Density at the surface	$\Delta\rho_{top}$	3200	$kg\ m^{-3}$
Density contrast at CMB	$\Delta\rho_{cmb}$	4300	$kg\ m^{-3}$
Density of the core	ρ_{core}	12500	$kg\ m^{-3}$
Temperature on the surface	T_{top}	731	K
Temperature at CMB	T_{cmb}	3700	K
Reference temperature	T_{ref}	2215	K
Gravitational constant	G	6.67×10^{-11}	$N\ m^2\ kg^{-2}$
Rate of internal heating	Q_v	7.5×10^{-9}	$W\ m^{-3}$
Clapeyron slope	γ	-2.8×10^6	$Pa\ K^{-1}$
Density jump at 730 km	$\Delta\rho_{730}$	390	$kg\ m^{-3}$

In our 3D models viscosity only varies with depth. Besides the viscosity Profile A based on *Pauer et al. (2006)* we also use three simple viscosity stratifications: constant viscosity mantle (B), Model C with linearly increasing viscosity and Model D with a high viscosity lithosphere underlain by an isoviscous mantle (Fig. 1). In some cases we carried out simulations in the spherical axisymmetric models which will be refered as 2D models. In these models we added lateral variations of viscosity on top of the depth variations of Profiles A–D. These lateral variations of viscosity follow Frank-Kamenetskii approximation of the temperature dependence (e.g. *Reese et al., 1999*):

$$\eta = \eta_{UM}\,\eta'(r)\exp\left[-\ln c\,\frac{T - T_{ref}}{T_{cmb} - T_{top}}\right]. \tag{7}$$

Here η_{UM} is a constant (its choice controls the *Ra*), $\eta' = \eta'(r)$ is a dimensionless reference viscosity at radius r (Profiles A–D), T_{ref} is the reference temperature and c is a non-dimensional parameter that controls an additional temperature induced viscosity contrast between the top and bottom surfaces.

For the values of the used parameters see Table 1. The list of the models is in Table 2.

We apply a semi-spectral method to solve the set of Eqs.(1)–(5) with the appropriate boundary conditions - the spherical harmonic decomposition laterally and finite differences in radius (*Čížková and Čadek, 1997*). Radial derivatives in the heat transport

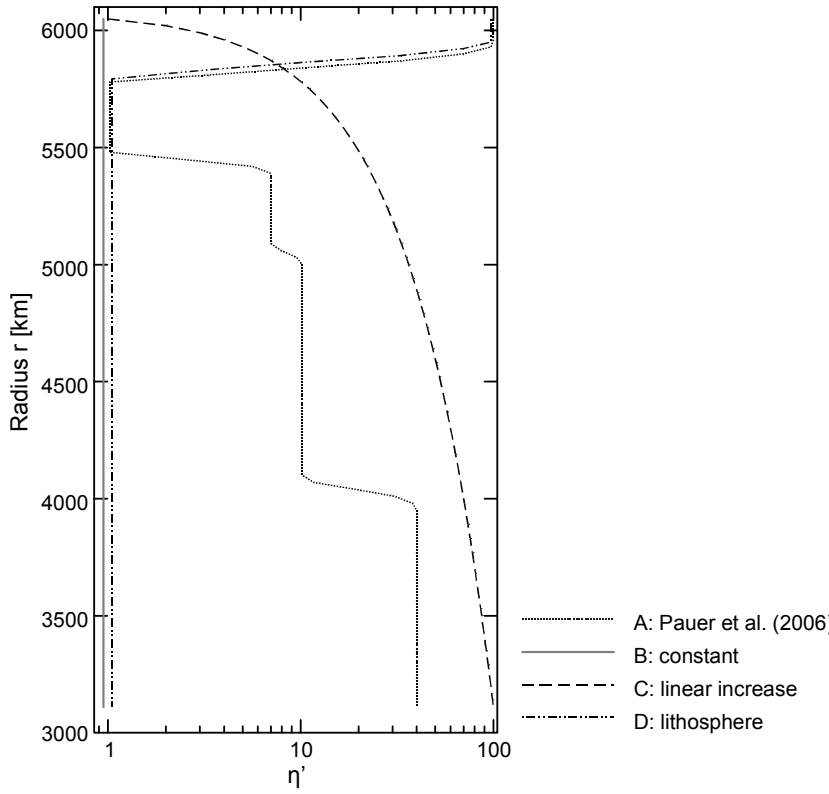

Fig. 1. Four profiles of the radially dependent dimensionless viscosity $\eta'(r)$ used in this study.

equation (3) are approximated using the Fornberg procedure (*Fornberg, 1988*). To integrate the equation we use a second order Runge-Kutta scheme - the Euler method. The non-linear terms $v \cdot \nabla T$, $v_r T$ and $\sigma : \nabla v$ in Eq.(3) are evaluated on a spatial grid (*Martinec, 1989*). Solution of the momentum equation was benchmarked against a spectral-finite element code (*Tosi and Martinec, 2007*). Both radial and lateral resolution varies among individual models depending on *Ra*, viscosity stratification, and the presence of the lateral variations of viscosity. Typically, the cut-off degree of the spherical harmonic expansion is between 170 and 250 and the radial resolution is about 10 to 30 km.

3. DATA

As the observed data we use the model of the Venus' geoid by *Konopliv et al. (1999)* and the topography model by *Rappaport et al. (1999)*. The power spectra of both geoid and topography plotted in a log-log scale show two changes of the slope - a more

Table 2. List of presented models. $\eta' = \eta'(r)$ denotes radial viscosity profile (see Fig. 1), η_{UM} is the upper mantle viscosity (η_{UM} corresponds to $\eta' = 1$ in Fig. 1), *Ra* is Rayleigh number and IH denotes if there is or is not included internal heating in the model.

	η'	η_{UM} [Pa s]	*Ra*	IH
3D Models				
3A8 × 10^{20}	*Pauer et al. (2006)*	8 × 10^{20}	7 × 10^{6}	no
3A2 × 10^{21}		2 × 10^{21}	2.8 × 10^{6}	
3A6 × 10^{21}		6 × 10^{21}	9 × 10^{5}	
3A3 × 10^{22}		3 × 10^{22}	2 × 10^{5}	
3A5 × 10^{22}		5 × 10^{22}	1 × 10^{5}	
3A2 × 10^{21}IH		2 × 10^{21}	2.8 × 10^{6}	yes
3B5 × 10^{21}	constant	5 × 10^{21}	2.61 × 10^{7}	no
3B4 × 10^{22}		4 × 10^{22}	3.3 × 10^{6}	
3B1 × 10^{23}		1 × 10^{23}	1.3 × 10^{6}	
3C1 × 10^{21}	linear increase	1 × 10^{21}	3 × 10^{6}	no
3C3 × 10^{21}		3 × 10^{21}	1 × 10^{6}	
3C5 × 10^{21}		5 × 10^{21}	6 × 10^{6}	
3C3 × 10^{22}		3 × 10^{22}	1 × 10^{6}	
3D4 × 10^{21}	lithosphere	4 × 10^{21}	6.1 × 10^{6}	no
3D5 × 10^{21}		5 × 10^{21}	4.9 × 10^{6}	
3D1 × 10^{22}		1 × 10^{22}	2.5 × 10^{6}	
3D5 × 10^{22}		5 × 10^{22}	5 × 10^{5}	
2D Models				
8 models with varying *Ra*	*Pauer et al. (2006)*	1 × 10^{20}–5 × 10^{23}	1 × 10^{4}–5.48 × 10^{7}	no
2A2 × 10^{21}	*Pauer et al. (2006)*	2 × 10^{21}	2.8 × 10^{6}	no
2A2 × 10^{21}IH				yes
2B4 × 10^{22}	constant	4 × 10^{22}	3.3 × 10^{6}	no
2B4 × 10^{22}IH				yes
2C5 × 10^{21}	linear	5 × 10^{21}	6 × 10^{5}	no
2C5 × 10^{21}IH				yes
2D1 × 10^{22}	lithosphere	1 × 10^{22}	2.5 × 10^{6}	no
2D1 × 10^{22}IH				yes
2A2 × 10^{21}LV0	*Pauer et al. (2006)*			yes
2A2 × 10^{21}LV1				
2A2 × 10^{21}LV2				
2A2 × 10^{21}LV3				

prominent one at about the degree of 40 and a slightly less pronounced but still significant one around the degree of 10 (*Pauer et al. 2006*). It has been hypothesised that the change of the slope at degree 40 is related to the change of the mechanism maintaining the geoid (topography) anomalies - the geoid of Venus is probably of a predominantly dynamic origin up to the degree 40. In this paper, we will therefore restrict observed and model geoid and topography analysis to the spectral range 3–40 (skipping the anomalous degree 2).

In order to measure the agreement between the observed and predicted data we introduce the quantity L_2d to evaluate the difference between the spectra in L_2 norm sense. Instead of comparing directly the power on individual degrees, we rather look at the slope of the geoid spectrum (*Čížková et al., 1996*). The slope should be characteristic for a given dynamic model and is less affected by the errors of individual degrees. Since the observed log-log spectra change the slope at the degree 10, we can characterise each model by two logarithmic slopes - one for degree range 3–9 and the other one for degrees 10–40. We are, however, interested not only in the slopes but also in the amplitudes. Therefore we approximate the decaying log-log spectra by two linear regression lines ($l^{3-9}(j)$ for degrees 3–9 and $l^{10-40}(j)$ for degrees 10–40) and then calculate the difference between these linear functions of the predicted and observed geoid. The L_2 norm difference L_2d is then defined as:

$$L_2d = \sqrt{\frac{\sum_{j=3}^{9}\left(l_{obs}^{3-9}(j) - l_{pred}^{3-9}(j)\right)^2 + \sum_{j=10}^{40}\left(l_{obs}^{10-40}(j) - l_{pred}^{10-40}(j)\right)^2}{38}}, \tag{8}$$

where $l_{obs}^{*}(j)$ and $l_{pred}^{*}(j)$ are the linear aproximations of the observed and predicted spectra, respectively. The L_2d is normalised by the number of degrees, thus giving an average difference (L_2d equal to 1 means that the observed and predicted spectra have one order of magnitude difference on average). Similarly, the L_2d difference is calculated also for the topography.

Besides the power spectra, we also compare the shape of the geoid and the topography anomaly above the plume developed on the pole of our 2D axisymmetric model with several topographic rises on Venus. About dozen of the Venus' rises are often interpreted by underlying thermal upwellings (*Stofan and Smrekar, 2005*; *Smrekar et al., 2010*). We have chosen four upwellings - Atla, Beta, West Eistla and Themis Regio. In order to compare the observed rises with the axially symmetric ones in 2D models, we average the observed anomalies to get an axisymmetric shape. The degree range is chosen according to the diameter of the Regios (j = 10–40) in order to avoid long-wavelength shift. The difference between the observed and predicted data is evaluated using the following quantity:

$$A_v d = \frac{\int_\theta \left| g_{obs}(\theta) - g_{pred}(\theta) \right| \mathrm{d}\theta}{\int_\theta \left| g_{obs}(\theta) \right| \mathrm{d}\theta}, \tag{9}$$

where $g_{obs}(\theta)$ and $g_{pred}(\theta)$ are observed and predicted geoid, respectively. θ is the co-latitude measured with respect to the centre of the plume and integration range is 0 to 10 degrees, respecting the diameter of the Regio. The $A_v d$ equal to 0.1 gives a 10% difference between the observed and predicted data, $A_v d$ of 1 means, that the observed and predicted data differ by 100%. Similarly, $A_v d$ is defined for topography.

4. RESULTS

First let us discuss the results of the 3D models. For each model, we have a time series of about 1 Gyr in a statistically steady-state (mean Nusselt number at both surface and core mantle boundary does not change with time). Before analysing these results we should check how much do the spectra change with time and whether one time snapshot can be representative of a given model. In cases of 3D models we found that though the flow pattern changes with time in all model cases, the character of the spectra - its slope on both long and intermediate wavelengths - is quite stable and the conclusions drawn on the basis of one snapshot in steady-state are the same, if we take another time snapshot.

Though the geoid undulations are only dependent on the radial variations of the viscosity and not on its absolute value, the latter one defines the Rayleigh number and thus the convection vigour and the character of the density anomalies. Therefore, it affects the geoid considerably. In Fig. 2 we demonstrate the sensitivity of the geoid and topography to the Rayleigh number. We vary the upper mantle viscosity η_{UM} in the range 8×10^{20}–1×10^{23} Pa s while holding other parameters fixed, so changing Rayleigh number in the range 9×10^4–2.6×10^7. We show here the $L_2 d$ difference between the predicted and observed spectra (Eq.(8)). Clearly, the spectra are sensitive to the upper

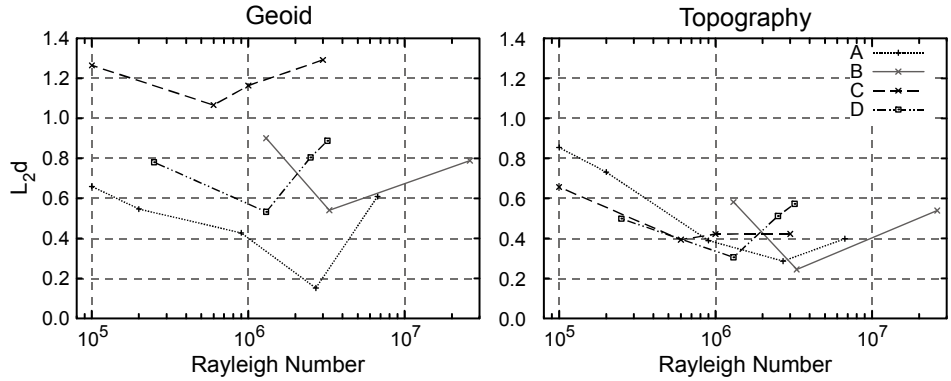

Fig. 2. The difference $L_2 d$ between the observed and predicted geoid (left panel) and topography (right panel) for four viscosity profiles as a function of the Rayleigh number. The results at one time instant are shown, but as the slope of the spectra is very stable with time in case of the 3D models, the figure looks very similar for any time instant in the statistically steady state. Line type coding is the same as in Fig. 1.

mantle viscosity (Rayleigh number). The preferred value of Rayleigh number is usually found around 10^6 (η_{UM} varies between 10^{21} and 10^{22} Pa s). For each viscosity profile (A–D) we thus obtain one model with best fit in the sense of $L_2 d$. In case of the viscosity Profile A, the best fit is obtained for a model 3A2 × 10^{21} with the upper mantle viscosity $\eta_{UM} = 2 \times 10^{21}$ Pa s (average $Ra = 3 \times 10^6$). The best fitting constant viscosity model 3B4 × 10^{22} has $\eta_{UM} = 4 \times 10^{22}$ Pa s ($Ra = 3 \times 10^6$). Linearly increasing viscosity (Model 3C5 × 10^{21}) produces the best fit for the $\eta_{UM} = 5 \times 10^{21}$ Pa s (average $Ra = 6 \times 10^5$). Finally Profile D with a stiff lithosphere prefers the upper mantle viscosity of $\eta_{UM} = 1 \times 10^{22}$ Pa s with average $Ra = 1 \times 10^6$ (Model 3D1 × 10^{22}).

Fig. 3 shows the geoid (top left panel) and topography (top right panel) spectra of best fitting models for each viscosity profile (A–D). Black line gives the spectra of the observed quantities. Let's look at the geoid first. Both Models B and D (grey and dash-dotted lines) overestimate observed geoid by about half an order of magnitude. Model C (dashed line) is succesful at long wavelengths (degrees 3 and 4) but then deviates from the observed spectrum and underestimates the signal. Clearly, as for the geoid, the best fitting

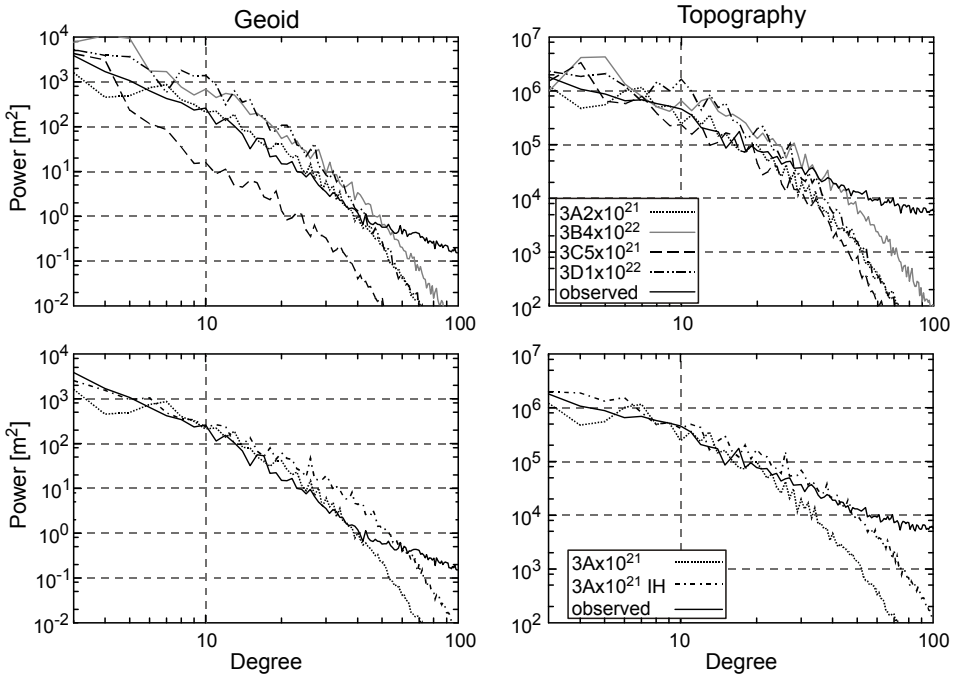

Fig. 3. Power spectra of the geoid (left) and topography (right) of Venus. Top panels show results for four different viscosity profiles - each for its ideal Rayleigh number. Line coding is the same as in Fig. 1. Bottom panels show the model 3A2 × 10^{21} (dotted) without internal heating and phase transition and model 3A2 × 10^{21}IH with phase transition and internal heating (dash-dotted). Black line shows the spectrum of the observed data.

model is A that explains the the observed data at degrees 5–40 very well. Let's now look at topography. Although Models B and D have slightly better fit for topography than geoid, they still overestimate observed data. Both Models A and C correspond with data quite well up to degreee 20.

Bottom panels of Fig. 3 show the effects of phase transition and internal heating. Dotted lines shows the Model 3A2 $\times 10^{21}$ without phase transitiv and internal heating, dash-dotted line is for the model that incorporates both effects. Clearly including the internal heating that supresses the plume activity improves the fit to topography at intermediate wavelengths but decreases the geoid fit. The differences between the purely bottom heated case and the model partly heated from within are however not strikingly high.

Above degree 40 the predicted spectral slope does not correspond for any model. At about that degree the slope of the observed geoid and topography changes, thus indicating that possibly different mechanisms are responsible for the generation of the geoid and topography on the shorter wavelengths. That is in agreement with the hypothesis, that the long wavelength part of the geoid and topography have purely dynamic source, while above the degree of 40 they are of a predominantly lithospheric origin (*Pauer et al., 2006*).

One representation of the convection planform for each of the four above mentioned models is shown in Fig. 4 (each of them for the same time instant as the spectra in Fig. 3). The Model 3D1 $\times 10^{22}$ with the constant viscosity under the stiff lithosphere (Fig. 3d) has a rather warm mantle and thus is characterised by a vigorous plume activity, with the total number of plumes of about 30. That is probably too much - there should be about 10 major plumes on Venus (*Smrekar and Parmentier, 1996*; *Smrekar et al., 2010*). Models A–C are generally in agreement with that criterion.

Let us now look at the 2D results. First, we should note, that the 2D spectra of the geoid and the topography have different character than the previously discussed spectra in the 3D models. The spectra in 2D models are much more oscillatory and contrary to the 3D models they vary with time considerably. Therefore rather than one value we will mostly be showing time average with standard deviation taken over the whole calculation (in a statistically steady-state).

Fig. 5 (similarly to Fig. 2) shows the sensitivity of the geoid and topography to the Rayleigh number. It depicts the $L_2 d$ difference between the observed and predicted spectra for the viscosity Profile A. Similarly to the 3D models (cf. Fig. 2), the best fit is obtained for the Rayleigh number of about 3×10^6. Such correspondence between the 2D and 3D results may suggest, that the plumes indeed are the features controlling the style of the flow and therefore a 2D approximation could be used to describe the basic character of the flow.

Fig. 6 demonstrates the effect of internal heating. We have 10 models with different parameters (viscosity profile, Rayleigh number) without internal heating and 10 corresponding models where internal heating was included. Majority of points is accumulated under black identity line which means that addition of internal heating effect generally improves the fit of our models. The effect is larger when looking at topography - almost all models (except one) have better fit of topography when internal heating is

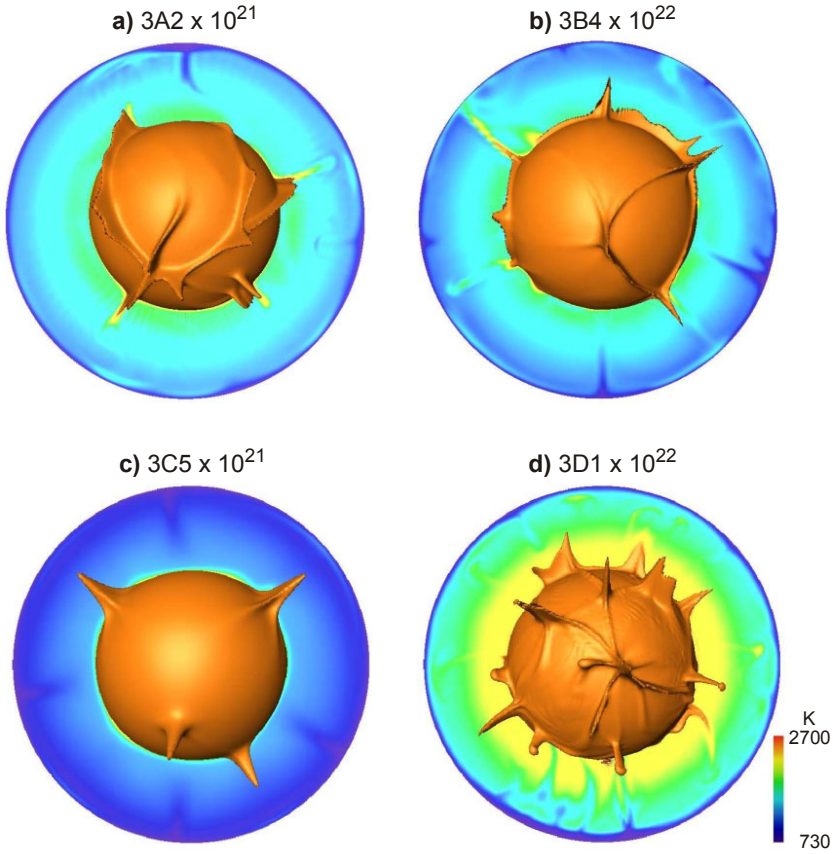

Fig. 4. Snapshots of the temperature field in four convection models: **a)** with the viscosity Profile A ($3A2 \times 10^{21}$), **b)** with Profile B ($3B4 \times 10^{22}$), **c)** with Profile C ($3C5 \times 10^{21}$) and **d)** with Profile D ($3D1 \times 10^{22}$). Shown isosurface corresponds to a temperature of 2500K.

included, while effect on geoid is not so obvious. Some models have even worse fit with internal heating. That is in accordance with the result of 3D model runs (Fig. 3).

Further, we tested the effect of the laterally variable viscosity. We had four models 2DALV0-3 with the depth viscosity stratification of Model A, but now the viscosity varies also laterally by 0–3 orders of magnitude with the temperature (see Eq.(7) - parameter $c = 1, 10, 100, 1000$). Clearly, the moderate lateral variations of viscosity do not improve the fit to the observed geoid and topography (Fig. 7).

Up to now, we used the power spectra of the geoid and the topografy as the only model output to be compared with the data. We will now look at another possible feature, that could be used to discriminate between the successful and unsuccessful models and

that is the actual shape of the geoid and topography above the assumed mantle plumes on Venus. Though there are certain doubts about the origin of some uplifted areas of the Venus' topography, others are generally believed to be associated with the mantle plumes. Among them the Atla and Beta Regio as well as Western Eistla, Bell, Thetis or Ovda Regio are often referenced in attempts to explain the geoid and the topography in the framework of the mantle convection models (*Kiefer and Hager, 1991*; *Smrekar and*

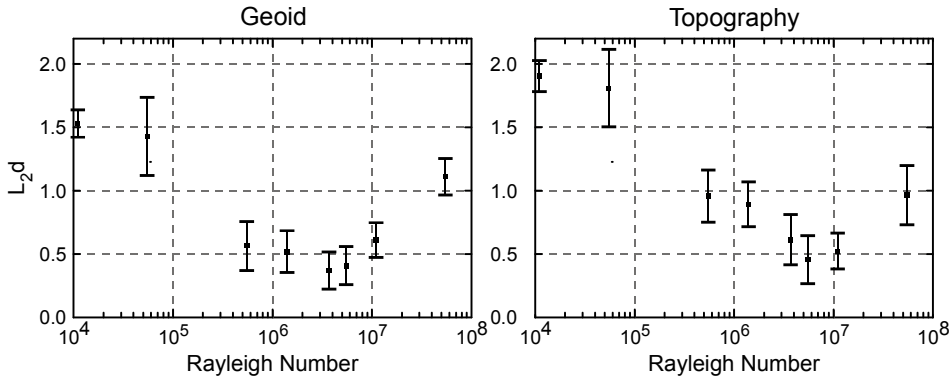

Fig. 5. The difference L_2d between the observed and predicted geoid **(a)** and topography **(b)** in a 2D model as a function of the Rayleigh number. The viscosity Profile A was used.

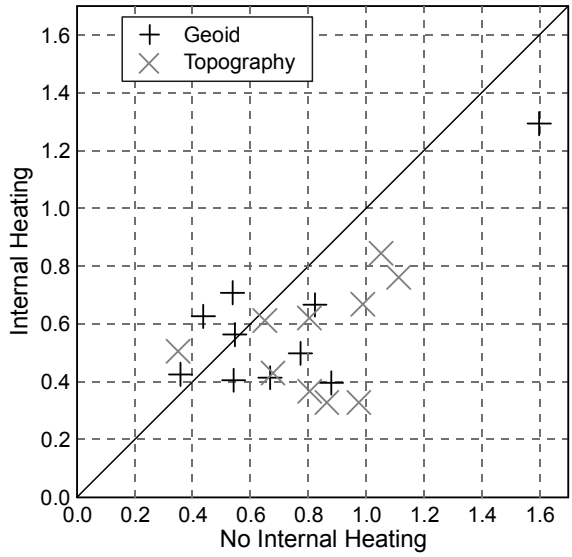

Fig. 6. Scatter plot shows the effect of internal heating. The difference L_2d in model without internal heating determines the position on the horizontal axis and the value of L_2d in model with internal heating determines the position on vertical axis.

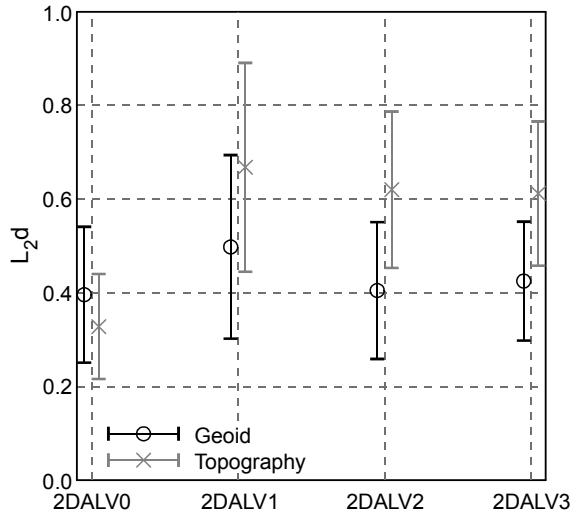

Fig. 7. The difference L_2d between the observed and predicted data in four models with increasing lateral variations of viscosity. The viscosity Profile A was used.

Phillips, 1991; *Smrekar and Parmentier, 1996*; *Solomatov and Moresi, 1996*; *Vezolainen et al., 2003*). We use here the data in four upwelling areas (Atla, Beta, West Eistla and Themis) and compare the shape of the anomalies with the topography and the geoid predicted in the polar plume area in our axisymmetric model. We have time evolution of 2 Gyr for four models (the most succesful for each viscosity profile - 2A2 $\times 10^{21}$IH, 2B4 $\times 10^{22}$IH, 2C5 $\times 10^{21}$IH and 2D1 $\times 10^{22}$IH) and we evaluate the $A_v d$ error (Eq.(9)) in each time instant. The $A_v d$ error is mostly high thus indicating a poor correspondence between the predicted and observed topography and geoid over the plume. At certain moments, however, this error drops and a quite good fit (less than 10% difference) of the observed and predicted geoid or topography is observed. The results are shown in Fig. 8, where we plot the histograms of the $A_v d$. When calculating the count, $A_v d$ of both the geoid and topography were assumed. First let us look on the left panel showing the histograms for four viscosity stratifications A (red), B (green), C (blue) and D (yellow). Each histogram includes the $A_v d$ of all four regios (Atla, Beta, Western Eistla and Themis). The succesful model characterised by a low $A_v d$ should have a count maximum at low $A_v d$. Clearly it is difficult to identify a really succesful model here as the moments with good fit are quite rare in all models. Model A may be considered the best, the count maximum at low $A_v d$ is however not very significant.

We should note here though, that the correspondence between the observed and predicted topography and geoid differs among the considered Regia. Our models are more succesful in explaining these quantities in Atla and Beta Regia, while for Western Eistla and Themis the fit is considerably lower. That is demonstrated in Fig. 8, on the right

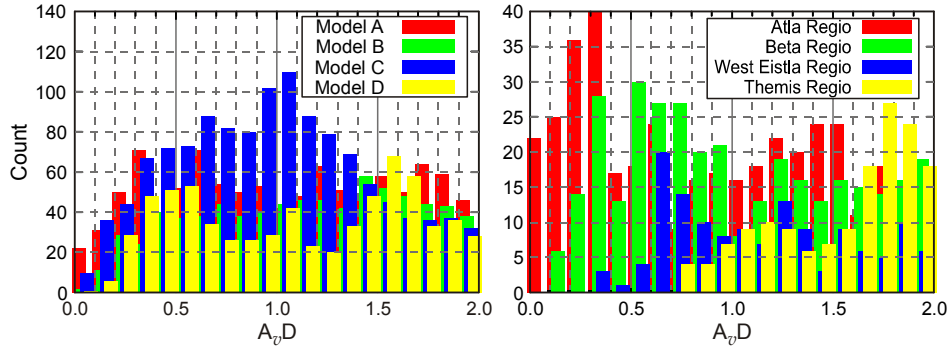

Fig. 8. Histograms illustrating the distribution of the $A_v d$ (difference between observed and modeled data). Counts on the vertical axis denote numbers of time instants giving appropriate $A_v d$ - the higher the count, the more often model reaches given $A_v d$ value. **Left:** comparison of four convection models based on Profiles A, B, C and D. Counts are sums for four regios (Atla, Beta, Western Eistla and Themis), both geoid and topography is considered. **Right:** distribution of the $A_v d$ values for individual regions. Only the most succesful Model A (both geoid and topography) is considered.

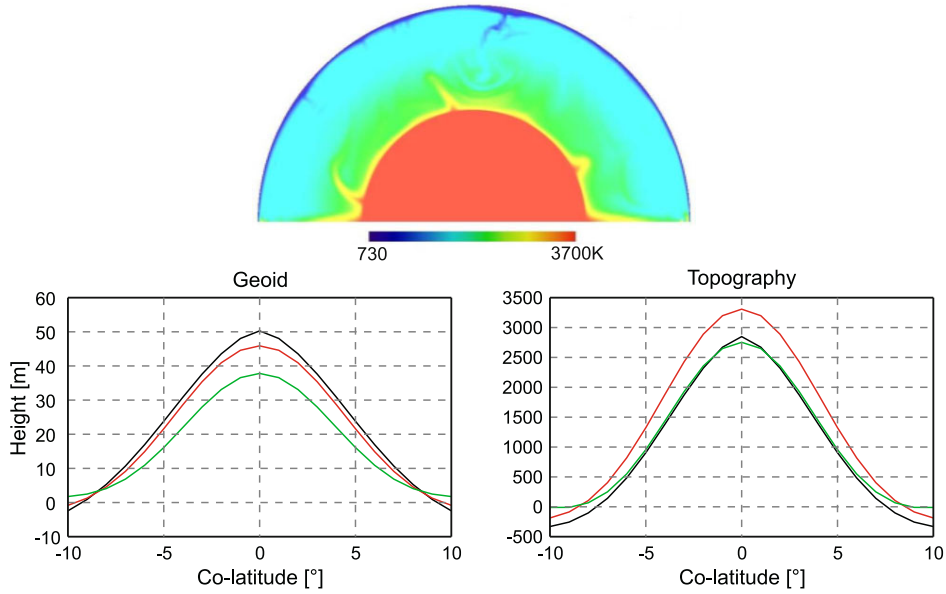

Fig. 9. **Top:** Temperature field of the best fitting 2D model at one time instant. **Bottom left:** Observed geoid in Atla Regio (black line) with the model prediction (Model 2A2 × 10^{21}IH). Green and red curves give the predictions in two different snapshots. Geoid and topography are calculated for degrees 10–40. **Bottom right:** The same, but for topography.

panel, where the histograms of $A_v d$ are shown for individual Regia and for the best fitting model $2A1 \times 10^{21}$IH. Fig. 9 illustrates the characteristic temperature distribution in the best fitting 2D model ($2A1 \times 10^{21}$IH) together with the observed geoid and topography in Atla Regio and the predicted quantities above the polar plume.

5. CONCLUSIONS

We used both 3D and 2D models of convection in the Venus' mantle in order to predict the dynamic topography and the geoid for various viscosity distributions. On the basis of combined evidence coming from the spectral fit, number of plumes developed in the mantle and the fit to the observed shape of the geoid and topography in several Regios on Venus, the Profile A characterised by a 200 km thick lithosphere followed by a gradual increase of viscosity with depth gives the best correspondence between the observed and predicted quantities. The best fitting model has the upper mantle viscosity of 2×10^{21} Pa s, thus giving an average Rayleigh number of 2.8×10^6. For all viscosity profiles the observed and predicted spectra coincide only up to the degree about 40. At higher degrees the slope of the predicted spectra differs from the observed ones considerably thus indicating other then dynamic origin of the geoid and topography anomalies.

While in 3D cases the spectra of the geoid and the topography are stable with time (the slope of the log-log spectrum varies only very weakly), in 2D models the spectra themselves are much more oscillatory and their slope oscillates quite wildly with time. Despite these differences, both 2D and 3D model runs prefer the same upper mantle viscosity. That may suggest, that the plumes are indeed the main dynamic features controlling the dynamic processes in the Venus' mantle and the 2D axisymmetric model provides its good approximation.

In the present work we assume that all topography is the result of convection motion (dynamic topography). As recently suggested by *Orth and Solomatov (2011)*, Venusian topography could be alternatively explained in terms of the thermal isostasy of the laterally variable stagnant lithosphere. The amplitude of the stagnant lid thickness variations however strongly depends on the convection model (e.g. internal vs. bottom heating, Newtonian vs. non-Newtonian viscosity). In some models the dynamic topography and geoid contribution due to the flow below the lid may be comparable or larger than the lithosphere contribution (*Solomatov and Moresi, 1997, 2000*). Our results could therefore be considered as an end-member case and the ratio of the stagnant lid thickness variations vs. convection induced topography should be subject to further research. In combination with these two mechanisms also the effects of the ratio of the internal and bottom heating should be tested in more detail.

The results of our 3D models are inevitably negatively influenced by the absence of the lateral variations of viscosity. We should note here however, that it has been shown by *Solomatov and Moresi (1996)*, that under the high viscosity stagnant lid the temperature variations are rather small and therefore also temperature induced lateral variations of viscosity may not play a key role. That is in a good agreement with the results of our 2D models, where the moderate temperature related lateral variations of viscosity do not improve the fit to the data. Further, *Tackley (1996)* pointed out, that the depth viscosity

variations play primary role in inuencing the dynamic regime of the mantle. Thus, though the thermally induced lateral variations of viscosity are potentially important in the 3D models due to the lithospheric thinning (*Solomatov and Moresi, 1996*; *Moore et al., 1999*), we believe, that our 3D results for a model with high viscosity lid should be able to describe the basic features of the Venus mantle dynamics.

Acknowledgements: We thank Nicola Tosi for fruitful discussions and for providing his data for benchmark of our code. Special thanks to Ondřej Čadek for numerous discussions and helpful comments. We thank Ana Negredo and an anonymous reviewer for the comments that helped to improve the manuscript. This research has been supported by the Grant Agency of Charles University grant No. GAUK 2333/2007, by the research project MSM0021620860 of the Czech Ministry of Education, Youth and Sports, and by grant SVV-2010-261308.

References

Arkani-Hamed J., 1996. Analysis and interpretation of the surface topography and gravitational potential of Venus. *J. Geophys. Res.*, **101**, 4711–4724.

Armann M. and Tackley P. J., 2010. 3-D spherical modelling of the thermo-chemical evolution of Venus' mantle and crust. *Geophys. Res. Abs.*, **12**, EGU2010-10507, 2010.

Barnett D.N., Nimmo F. and McKenzie D., 2002. Flexure of Venusian lithosphere measured from residual topography and gravity. *J. Geophys. Res.*, **107**, 5007, DOI: 10.1029/2000JE001398.

Běhounková M. and Choblet G., 2009. Onset of convection in a basally heated spherical shell, application to planets. *Phys. Earth Planet. Inter.*, **176**, 157–173.

Choblet G. and Sotin C., 2000. 3D thermal convection models of uids with variable viscosity: comparison between secular cooling and volumetric heating. *Phys. Earth Planet. Inter.*, **119**, 321–336.

Čížková H., Čadek O., Yuen D.A. and Zhou H., 1996. Slope of geoid spectrum and constraints on mantle viscosity stratification. *Geophys. Res. Lett.*, **23**, 3063–3066.

Čížková H. and Čadek O., 1997. Effect of a viscosity interface at 1000 km depth on mantle convection. *Stud. Geophys. Geod.*, **41**, 297–306.

Dubuffet F., Rabinowicz M. and Monnereau M., 2000. Multiple scales in mantle convection. *Earth Planet. Sci. Lett.*, **178**, 351–366.

Fornberg B., 1988. Generation of finite-difference formulas on arbitrarily spaced grids. *Math. Comput.*, **51**, 699–706.

Kiefer W.S., Richards M.A., Hager B.H. and Bills B.G., 1986. A dynamic-model of Venus gravity field. *Geophys. Res. Lett.*, **13**, 14–17.

Kiefer W.S. and Hager B.H., 1991. A mantle plume model for the Equatorial Highlands of Venus. *J. Geophys. Res.*, **96**, 20947–20966.

Kiefer W.S. and Kellogg L.H., 1998. Geoid anomalies and dynamic topography from time-dependent, spherical axisymmetric mantle convection. *Phys. Earth Planet. Inter.*, **106**, 273–256.

King S.D., 1997. Geoid and topographic swells over temperature-dependent thermal plumes in spherical-axisymmetric geometry. *Geophys. Res. Lett.*, **24**, 3093–3096.

Konopliv A.S., Banerdt W.B. and Sjogren W.L., 1999. Venus gravity: 180th degree and order model. *Icarus*, **139**, 3–18.

Martinec Z., 1989. Program to calculate the spectral harmonic expansion coefficients of the two scalar fields product. *Comput. Phys. Commun.*, **54**, 177–182.

Matyska C. and Yuen D.A., 2007. Lower mantle material properties and convection models of multiscale plumes. In: Foulger G.R. and Jurdy D.M. (Eds.), *Plates, Plumes and Planetary Processes*. Special Paper 430. The Geological Society of America, Boulder, CO, 137–163.

Moore W.B., Schubert G. and Tackley P.J., 1999. The role of rheology in lithospheric thinning by mantle plumes. *Geophys. Res. Lett.*, **26**, 1073–1076.

Orth C.P. and Solomatov V.S., 2011. The isostatic stagnant lid approximation and global variations in the Venusian lithospheric thickness. *Geochem. Geophys. Geosyst.*, **12**, Q07018.

Pauer M., Fleming K. and Čadek O., 2006. Modeling the dynamic component of the geoid and topography of Venus. *J. Geophys. Res.*, **111**, E11012.

Rappaport N.J., Konopliv A.S. and Kucinskas A.B., 1999. An improved 360 degree and order model of Venus topography. *Icarus*, **139**, 19–31.

Ratcliff J.T., Schubert G. and Zebib A., 1995. 3-dimensional variable viscosity convection of an infinite Prandtl number Boussinesq fluid in a spherical-shell. *Geophys. Res. Lett.*, **22**, 2227–2230.

Reese C.C., Solomatov V.S., Baumgardner J.R. and Yang W.S., 1999. Stagnant lid convection in a spherical shell. *Phys. Earth Planet. Inter.*, **116**, 1–7.

Schubert G., Solomatov V.S., Tackley P.J. and Turcotte D.L., 1997. Mantle convection and the thermal evolution of Venus. In: Bougher S.W., Hunten D.M. and Phillips R.J. (Eds.), *Venus II - Geology, Geophysics, Atmosphere, and Solar Wind Environment*. University of Arizona Press, Tucson, Arizona, 1245–1288.

Schubert G., Turcotte D.L. and Olson P., 2001. *Mantle Convection in the Earth and Planets*. Cambridge University Press, New York.

Simons M., Hager B.H. and Solomon S.C., 1994. Global variations in the geoid/topography admittance of Venus. *Science*, **264**, 798–803.

Smrekar S.E. and Parmentier E.M., 1996. The interaction of mantle plumes with surface thermal and chemical boundary layers: Applications to hotspots on Venus. *J. Geophys. Res.*, **101**, 5397–5410.

Smrekar S.E. and Phillips R.J., 1991. Venusian highlands - geoid to topography ratios and their implications. *Earth Planet. Sci. Lett.*, **107**, 582–597.

Smrekar S.E., Stofan E.R., Mueller N., Treiman A., Elkins-Tanton L., Helbert J., Piccioni G. and Drossart P., 2010. Recent hotspot volcanism on Venus from VIRTIS emissivity data. *Science*, **328**, 605–608.

Solomatov, V. S., Moresi, L. N., 1996. Stagnant lid convection on Venus. J. Geophys. Res., 101, 4737-4753.

Solomatov V.S. and Moresi L.N., 1997. Three regimes of mantle convection with non-Newtonian viscosity and stagnant lid convection on the terrestrial planets. *Geophys. Res. Lett.*, **24**, 1907–1910.

Solomatov V.S. and Moresi L.N., 2000. Scaling of time-dependent stagnant lid convection: Application to small-scale convection on Earth and other terrestrial planets. *J. Geophys. Res.*, **105**, 21795–21817.

Steinbach V. and Yuen D.A., 1994. Effects of depth-dependent properties on the thermal anomalies produced in flush instabilities from phase transitions. *Phys. Earth Planet. Inter.*, **86**, 165–183.

Steinbach V. and Yuen D.A., 1998. The influences of surface temperature on upwellings in planetary convection with phase transitions. *Earth Planet. Sci. Lett.*, **162**, 15–25.

Steinberger B., Werner S.C. and Torsvik T.H., 2010. Deep versus shallow origin of gravity anomalies, topography and volcanism on Earth, Venus and Mars. *Icarus*, **207**, 564–577.

Stofan E.R. and Smrekar S.E., 2005. Large topographic rises, coronae, large flow fields, and large volcanoes on Venus: Evidence for mantle plumes? In: Foulger G.R. and Jurdy D.M. (Eds.), *Plates, Plumes and Planetary Processes*. Special Paper 338. The Geological Society of America, Boulder, CO, 841–861.

Tackley P.J., 1993. Effects of strongly temperature-dependent viscosity on time-dependent, 3-dimensional models of mantle convection. *Geophys. Res. Lett.*, **20**, 2187–2190.

Tackley P.J., 1996. Effects of strongly variable viscosity on three-dimensional compressible convection in planetary mantles. *J. Geophys. Res.*, **101**, 3311–3332.

Tosi N. and Martinec Z., 2007. Semi-analytical solution for viscous Stokes flow in two eccentrically nested spheres. *Geophys. J. Int.*, **170**, 1015–1030.

Vezolainen A.V., Solomatov V.S., Head J.W., Basilevsky A.T. and Moresi L.N., 2003. Timing of formation of Beta Regio and its geodynamical implications. *J. Geophys. Res.*, **108**, 5002, DOI: 10.1029/2002JE001889.

Yoshida M. and Kageyama A., 2006. Low-degree mantle convection with strongly temperature- and depth-dependent viscosity in a three-dimensional spherical shell. *J. Geophys. Res.*, **111**, B03412.